The influence of erosion thresholds and runoff variability on the relationships among topography, climate, and erosion rate

Roman A. DiBiase[1] and Kelin X. Whipple[1]

Received 18 May 2011; revised 20 October 2011; accepted 24 October 2011; published 29 December 2011.

[1] Bedrock river incision occurs only during floods large enough to mobilize sediment and overcome substrate detachment thresholds. New data relating channel steepness and erosion rate provide the opportunity to evaluate the role of thresholds and discharge variability in landscape evolution. We augment an extensive erosion rate data set in the San Gabriel Mountains, California, with analysis of streamflow records and observations of channel width and sediment cover to evaluate the importance of climate and erosion thresholds on incision rates. We find the relationship between channel steepness and erosion rate in the San Gabriel Mountains can be explained using a simple stochastic-threshold incision model where the distribution of large floods follows an inverse power law, suggesting that details of incision mechanics, sediment effects, width adjustment, and debris flows do not significantly influence the steady state relationship between steepness and erosion rate. Using parameters tuned to this case, we vary climate parameters to explore a range of behavior for the steepness-erosion relationship. Erosion is enhanced by both increases in mean runoff and discharge variability. We explore the implications of an empirical relationship between mean runoff and variability to test whether dry, variable climates can erode more efficiently than wet, stable climates. For channels with high thresholds or low steepness, modeled erosion rate peaks at a mean runoff of 200–400 mm/yr. For much of the parameter space tested, erosion rates are predicted to be insensitive to increases in runoff above ~500 mm/yr, with important implications for the hypothesized influence of climate on tectonics.

Citation: DiBiase, R. A., and K. X. Whipple (2011), The influence of erosion thresholds and runoff variability on the relationships among topography, climate, and erosion rate, *J. Geophys. Res.*, *116*, F04036, doi:10.1029/2011JF002095.

1. Introduction

[2] Understanding what controls erosion rate in mountainous terrain is critical to the study of a wide range of tectonic and geomorphic problems, such as exploring potential feedbacks between climate and uplift [*Hilley and Strecker*, 2004; *Roe et al.*, 2008; *Stolar et al.*, 2007; *Whipple*, 2009; *Willett*, 2010], determining the role of extreme versus frequent events in shaping the landscape [*Hartshorn et al.*, 2002; *Wolman and Miller*, 1960], and distinguishing between climatic and tectonic signals in sedimentary basin deposits [*Armitage et al.*, 2011; *Paola et al.*, 1992]. Bedrock rivers define the relief structure of unglaciated ranges, set the pace of hillslope denudation, and transmit changes in baselevel throughout the landscape. Accordingly, bedrock rivers have been a focus of considerable research over the past decade [e.g., *Cowie et al.*, 2008; *Gasparini et al.*, 2007; *Tucker and Hancock*, 2010; *Whipple*, 2004]. Existing models for bedrock river incision generally predict that erosion rate depends to first order on topographic relief, climate, lithology, and sediment caliber and flux; yet there is a dearth of field data that can be used to evaluate even the relative importance of these factors. For example, it was first recognized over a century ago that sediment in bedrock channels dually influences erosion by both providing tools to erode the bed and cover to protect it [*Gilbert*, 1877]. *Sklar and Dietrich* [1998, 2004] developed a bed load saltation-abrasion model that accounted for these effects, and much recent work has focused on refining and calibrating the exact formulations for both "tools" and "cover" effects. These adjustments have been primarily theoretical [*Lague*, 2010; *Lamb et al.*, 2008; *Turowski*, 2009], or based on laboratory flume experiments [*Chatanantavet and Parker*, 2008; *Johnson and Whipple*, 2010; *Sklar and Dietrich*, 2001]. In addition, the potential influence of channel narrowing in response to increased incision rate has likewise been the focus of several theoretical treatments [*Finnegan et al.*, 2007, 2005; *Stark*, 2006; *Turowski et al.*, 2007, 2009; *Wobus et al.*, 2006b, 2008; *Yanites and Tucker*, 2010]. In this regard, theory is far ahead of observation, and only recently have workers begun quantifying in the field the influence of tools and cover on bedrock incision

[1]School of Earth and Space Exploration, Arizona State University, Tempe, Arizona, USA.

0148-0227/11/2011JF002095

rates [e.g., *Cowie et al.*, 2008; *Jansen*, 2006; *Jansen et al.*, 2011; *Johnson et al.*, 2009; *Tomkin et al.*, 2003; *Valla et al.*, 2010]. Furthermore, the predicted steady state channel profiles of detachment-limited and sediment-flux dependent channels mimic those of the transport-limited case, and only during transient conditions are the differences between these formulations observable [e.g., *Attal et al.*, 2011; *Gasparini et al.*, 2007; *Valla et al.*, 2010]. This result deemphasizes the influence of fully incorporating sediment flux relations into steady state models. In this paper, we return to work done by *Tucker and Bras* [2000], *Snyder et al.* [2003b], *Tucker* [2004], and *Lague et al.* [2005], and argue that under steady state conditions and spatially uniform erosion rate, the effects of dynamic width adjustment and sediment cover are subordinate to the role of erosion thresholds and discharge variability in controlling the relation between topography and bedrock channel incision rate. Specifically our field data show no evidence that width and sediment cover differ as a function of erosion rate under steady state, uniform rock uplift conditions and we demonstrate that a simple stochastic-threshold model [*Lague et al.*, 2005] can explain the observed relationship between channel steepness and erosion rate without appeal to a tools/cover effect or dynamic channel width adjustment.

[3] A number of recent studies attempted to isolate the topographic controls on erosion rates by investigating landscapes where climate and lithology are nearly uniform. *DiBiase et al.* [2010] and *Ouimet et al.* [2009] used cosmogenic ^{10}Be concentrations in active stream sediments to quantify millennial erosion rates for comparison with the channel steepness index, a metric of fluvial relief that normalizes local channel slope for its expected dependence on drainage area [*Wobus et al.*, 2006a]. They found that the channel steepness index increases monotonically with catchment-averaged erosion rate for equilibrium channels (those lacking distinct knickpoints) in the San Gabriel Mountains [*DiBiase et al.*, 2010] and along the eastern margin of the Tibetan plateau [*Ouimet et al.*, 2009]. The channel steepness index emerges as a robust metric of topographic relief that reflects the influence of tectonics, climate, and lithology and that can furthermore be directly tied to bedrock incision models.

[4] While the distinction between specific transport-limited, detachment-limited, and sediment-flux dependent models of fluvial incision is often only expressed during transient landscape response [*Attal et al.*, 2011; *Gasparini et al.*, 2007; *Valla et al.*, 2010; *Whipple and Tucker*, 2002], the relief-erosion rate relationships for steady state conditions determined in the above studies allows for an examination of first order controls on channel steepness common to all incision models. For example, channel width variation, the presence of erosion thresholds, and water discharge magnitude and variability will all influence the shape of the relationship between relief and landscape-averaged erosion rate predicted by all variants of river incision models. Both *Ouimet et al.* [2009] and *DiBiase et al.* [2010] found a power law relation between channel steepness and erosion rate:

$$k_s \propto E^{\phi}, \tag{1}$$

where k_s is the channel steepness index, E is long-term erosion rate, and $\phi \sim 0.5$. The dimension of k_s depends on the assumed reference concavity, which we fix to 0.45, resulting in units of $m^{0.9}$ [*Wobus et al.*, 2006a]. In every studied region, channel steepness increases monotonically with increasing rates of base-level fall, as quantified by either erosion or rock uplift rate [*Cyr et al.*, 2010; *DiBiase et al.*, 2010; *Duvall et al.*, 2004; *Harkins et al.*, 2007; *Kirby and Whipple*, 2001; *Ouimet et al.*, 2009; *Safran et al.*, 2005; *Snyder et al.*, 2003b; *Wobus et al.*, 2006a]. However, the magnitude and shape of this relationship varies widely among different field sites. For example, while a channel steepness index of 60 $m^{0.9}$ is sufficient to erode at 10 mm/yr in the Siwalik Hills of Nepal, one tenth that erosion rate requires a channel steepness of 500 $m^{0.9}$ along the eastern margin of the Tibetan plateau [*Ouimet et al.*, 2009; *Wobus et al.*, 2006a]. Furthermore, the shape of this relationship varies; studies have fit data to equation (1) with $\phi \sim 0.25$ [*Snyder et al.*, 2003b], $\phi \sim 0.5$ [*DiBiase et al.*, 2010; *Harkins et al.*, 2007; *Ouimet et al.*, 2009], and $\phi \sim 1$ [*Kirby and Whipple*, 2001; *Safran et al.*, 2005; *Wobus et al.*, 2006a]. For the cases where $\phi < 1$, the erosional efficiency of a channel, or its capacity to incise for a given slope, increases with erosion rate (or equivalently, slope).

[5] A nonlinear (i.e., $\phi < 1$) relationship between channel steepness and erosion rate may arise for a number of reasons. For example, the relationship between erosion and bed shear stress may be nonlinear, as in the case of suspended-load abrasion or plucking [*Whipple et al.*, 2000]; bedrock exposure may change with channel slope, either decreasing available sediment cover or increasing the amount of tools available to abrade the bed [*Sklar and Dietrich*, 2006]; orographic precipitation gradients may intensify rainfall in steeper catchments [*Roe et al.*, 2002]; channels may narrow as they steepen [*Finnegan et al.*, 2005; *Lavé and Avouac*, 2001; *Whittaker et al.*, 2007; *Wobus et al.*, 2006b; *Yanites and Tucker*, 2010]; or an erosion threshold may preferentially retard incision of low gradient channels [*Lague et al.*, 2005; *Snyder et al.*, 2003b; *Tucker*, 2004; *Tucker and Bras*, 2000]. Other factors, including the role of debris flows and varying bed roughness, may also contribute to steep channels becoming more efficient. The relative importance of all the factors listed above on the relation between channel steepness and erosion rate is, however, unclear.

[6] A successful model must include at least thresholds of motion and/or detachment and a representation of the stochastic distribution of floods, as these are known to operate in all channels, whether transport- or detachment-limited [*Lague et al.*, 2005; *Sklar and Dietrich*, 2006; *Snyder et al.*, 2003b; *Tucker*, 2004]. In this contribution, we ask whether a simple model incorporating these factors alone can explain the range of behavior observed in relationships between channel steepness and erosion rate under steady state and uniform rock uplift conditions. We begin with a review of the theoretical framework of published stochastic-threshold models that predict a nonlinear relationship between channel steepness (k_s) and erosion rate (E) consistent with equation (1), and then use these models and the erosion rate data set of *DiBiase et al.* [2010], along with detailed field surveys and discharge records, to explore the controls on ϕ in the San Gabriel Mountains of California. Finally, we combine the model of *Lague et al.* [2005] with an empirical relationship between discharge variability and mean runoff [*Molnar et al.*, 2006] to explore the influence of climate on

erosion rate as a function of channel steepness and erosion threshold magnitude.

2. Theoretical Framework

2.1. Overview of Stream Power Model

[7] We begin by reviewing the formulation of a generalized stream power incision model that incorporates both a threshold term and a stochastic distribution of flood discharges [*Lague et al.*, 2005; *Tucker and Bras*, 2000]. As we will discuss later, graded rivers in the San Gabriel Mountains are actively incising bedrock (at rates from 0.1 to 1 mm/yr), but tend to be mantled with a thin layer of alluvium. Here we follow *Lague et al.* [2005] in employing a detachment-limited model for simplicity. We acknowledge this as a limitation, but emphasize that at steady state under uniform rock uplift rate conditions the relationship between k_s and E predicted by detachment-limited, transport-limited, and sediment-flux dependent incision models are broadly similar, as shown by *Whipple and Tucker* [2002], *Tucker* [2004], *Sklar and Dietrich* [2006], and *Gasparini et al.* [2007]. In particular, *Tucker* [2004] showed that when the effects of thresholds for detachment or sediment mobilization and a stochastic distribution of floods are incorporated, end-member detachment- and transport-limited models predict nearly identical steady state relationships between k_s and E (see Figures 7a and 7c of *Tucker* [2004]); we surmise that steady state relationships among topography, thresholds, mean runoff, runoff variability, and erosion rate predicted by a detachment-limited model, as used here, will be broadly applicable. Thus, we will adopt the commonly used stream power model of detachment-limited channel incision, which postulates that instantaneous vertical channel incision I is proportional to a power law of bed shear stress τ, commonly approximated as

$$I = k_e\left(\tau^a - \tau_c^a\right), \tag{2}$$

where k_e and a are parameters that depend on substrate properties and erosion process, respectively [*Howard and Kerby*, 1983; *Lague et al.*, 2005; *Snyder et al.*, 2003b; *Tucker*, 2004]. The threshold term τ_c represents a critical shear stress which must be overcome before erosion occurs. At a minimum, τ_c must be large enough to mobilize detached particles or bed load material, and may be much larger in channels where plucking of fractured blocks is the dominant incision process [*Snyder et al.*, 2003b].

[8] Next we must describe how shear stress depends on water discharge both due to at-a-station variability and downstream increases. A common formulation involves combining a steady, uniform flow approximation for a wide channel (i.e., negligible bank friction) with a frictional resistance relationship (e.g., Manning, Darcy-Weisbach equations), to express bed shear stress as

$$\tau = k_t\left(\frac{Q}{w}\right)^{\alpha} S^{\beta}, \tag{3}$$

where k_t is a constant that incorporates gravitational and frictional terms, Q is water discharge, w is channel width, S is water surface slope (usually approximated by the channel bed gradient), and α and β are exponents that depend on the frictional relationship used (for a Manning relation, α = 3/5 and β = 7/10, and for a Darcy-Weisbach relation, $\alpha = \beta$ = 2/3; see *Howard* [1994] for full derivation). To close equation (3), we must explicitly model how channel width varies across the landscape. In lieu of a more rigorous and direct treatment, bedrock channel width is often modeled using classical hydraulic geometry relations originally developed for alluvial rivers and found to be good descriptors in bedrock rivers as well [e.g., *Montgomery and Gran*, 2001; *Wohl and David*, 2008]

$$w_b = k_w Q_b^{\omega_b}, \tag{4a}$$

$$\frac{w}{w_b} = \left(\frac{Q}{Q_b}\right)^{\omega_s}, \tag{4b}$$

where the subscript b indicates a reference condition such as mean daily or bankfull flow, and k_w, ω_b, and ω_s are typically empirically derived constants for downstream (equation (4a)) and at-a-station (equation (4b)) variations in channel width [*Tucker*, 2004].

[9] Combining equations (3) and (4), we can write bed shear stress as:

$$\tau = k_t k_w^{-\alpha}\left(\frac{Q}{Q_b}\right)^{\alpha(1-\omega_s)} Q_b^{\alpha(1-\omega_b)} S^{\beta}, \tag{5}$$

with the dependence on water discharge partitioned into at-a-station variation (Q/Q_b term) and downstream variation (Q_b term). Although ω_s is defined in equation (4b) as a function of channel cross-sectional geometry alone [e.g., *Turowski et al.*, 2008], it enters the bedrock channel erosion problem through its influence on the exponent on the at-a-station discharge variability term ($\alpha(1 - \omega_s)$) after being combined with a resistance relationship that ignores bank friction. We show in the auxiliary material that although ω_s, as defined in equation (4b), varies significantly as a function of channel cross-sectional geometry [*Turowski et al.*, 2008], tradeoffs between the increase in width with discharge in channels with gentle banks, and an increase in sidewall friction with discharge in channels with steep banks, conspire to hold the at-a-station discharge exponent ($\alpha(1 - \omega_s)$) approximately constant at $\sim$0.5 under a wide range of channel cross-sectional forms (see auxiliary material).[1] Given that $0.6 < \alpha < 0.7$ holds for standard resistance relationships and the cross-sectional flow model we use in the auxiliary material [*Kean and Smith*, 2004], we implement this constraint in our analyses by holding α fixed at 2/3 and ω_s fixed at 0.25, but acknowledge that this aspect of the problem merits further work.

[10] In many landscapes, it is reasonable to substitute a power law relationship between a characteristic discharge (such as the mean daily or bankfull) and upstream drainage area A, such that

$$Q_b = R_b A^c, \tag{6}$$

[1] Auxiliary materials are available in the HTML. doi:10.1029/2011JF002095.

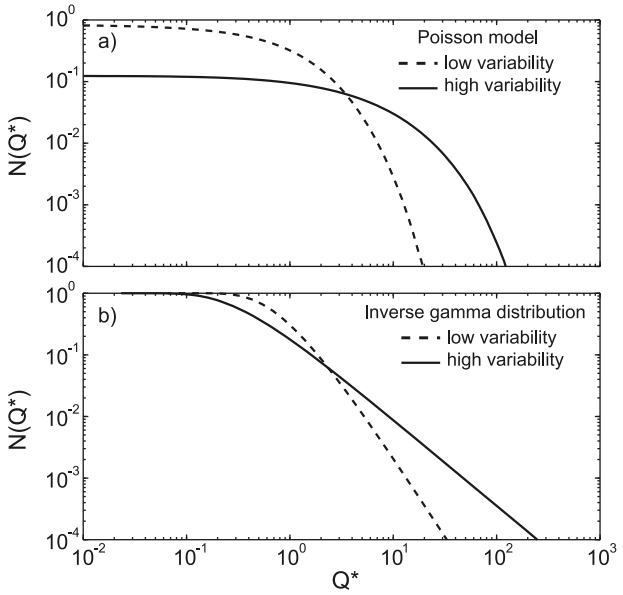

Figure 1. Plots of predicted exceedence frequency as a function of non-dimensional daily discharge for (a) the Poisson rainfall model and (b) the inverse gamma distribution discharge model. Poisson discharge distribution was calculated using a Monte Carlo approach to model individual storms and assumes simple Horton overland flow with negligible infiltration.

where R_b and c are again empirically derived constants. We define this characteristic discharge based solely on streamflow data, rather than channel form, and for our case in the San Gabriel Mountains, we find that $c \sim 1$, for both mean daily discharges (see section 3.2) and for decadal maximum flood events [*Lavé and Burbank*, 2004]. Thus R_b can be thought of as a characteristic runoff with dimensions of L/T [*Tucker*, 2004]. We use mean daily discharge as the reference discharge Q_b in all our analyses and thus R_b represents mean daily runoff. Finally, we can use a representation of the channel steepness index consistent with steady state channels and the stream power river incision model,

$$k_s = SA^{m/n}, \tag{7}$$

where $m = \alpha a(1 - \omega_b)$ and $n = \beta a$ to incorporate the topographic variables into a single term. The channel steepness index k_s, can be readily derived from digital elevation models, and for steady state landscapes serves as a scale-independent metric of fluvial relief [*DiBiase et al.*, 2010; *Wobus et al.*, 2006a]. Using equations (5) and (7), instantaneous channel incision (equation (2)) can be written as

$$I = K\left(\frac{Q}{Q_b}\right)^{\gamma} k_s^n - \Psi, \tag{8}$$

where $K = k_e k_t^a k_w^{-\alpha a} R_b^m$, $\gamma = \alpha a(1 - \omega_s)$, and $\Psi = k_e \tau_c^a$. Equation (8) represents the simplest formulation that, when combined with a probability distribution of flood discharges, allows for the study of climatic influences on fluvial incision as a function of topography. Versions of equation (8) are used by *Tucker and Bras* [2000], *Snyder et al.* [2003b], *Tucker* [2004], and *Lague et al.* [2005].

2.2. Discharge Variability and Long-Term Erosion Rate

[11] For a given channel reach, equation (8) predicts a power law relationship between instantaneous bedrock incision rate and water discharge. A similar power law relationship is commonly used to model bed load transport [e.g., *Bagnold*, 1977; *Meyer-Peter and Müller*, 1948]. *Wolman and Miller* [1960] combined such a relationship with an assumed lognormal distribution of annual peak flows to introduce the concept of an effective discharge that defines channel morphology; small flows do not perform enough work, and large floods are too infrequent. Often the effective discharge in alluvial channels is assumed to be roughly equivalent to the bankfull flood (recurrence interval ~1–2 years). This conceptual framework has transferred to studies of bedrock rivers, where in most studies Q in equation (7) is set to a reference discharge Q_b, and τ_c is assumed to be insignificant during such flows. This gives the familiar expression for long-term channel erosion E [*Whipple and Tucker*, 1999],

$$E = K' A^m S^n. \tag{9}$$

If using the assumption of $Q = Q_b$, as done in the standard stream power model, the dynamic impact of including the threshold term Ψ becomes absorbed into the constant K'. However, in order to appreciate the influence of the threshold term Ψ, equation (8) must be paired with a model of temporal variability of flood discharge because the fraction of time that flows exceed the threshold is a key factor in long-term erosion [*Lague et al.*, 2005; *Snyder et al.*, 2003b; *Tucker*, 2004].

[12] *Tucker and Bras* [2000], *Tucker* [2004], and *Lague et al.* [2005] instead defined Q as a probability density function $pdf(Q)$, and show that the long-term erosion rate E is given by the product of instantaneous incision rate for a given discharge and the probability of a flood of that magnitude, integrated over the full distribution of floods,

$$E = \int_{Q_c(k_s)}^{Q_m} I(Q, k_s) pdf(Q) dQ, \tag{10}$$

where Q_c is the discharge needed to overcome the threshold shear stress and Q_m is the maximum discharge considered. *Lague et al.* [2005] showed that for most of parameter space (and for all cases considered in this study), the integral in equation (10) converges quickly and the choice of Q_m is insignificant for $Q_m/Q_b > 100$. Q_c can be determined by setting I in equation (8) to zero and solving for Q. Importantly, Q_c varies with the channel steepness index, k_s (gentler channels require larger flows to overcome erosion thresholds), introducing complexity to the relationship between E and k_s. The nature of the resulting relationship depends on the nature of the probability density function $pdf(Q)$ in equation (10). *Tucker and Bras* [2000] and *Tucker* [2004] used the Poisson pulse storm rainfall model of *Eagleson* [1978], along with a simple hydrologic model (spatially uniform Horton overland flow), which together result in an exponential distribution of discharges (Figure 1a). In contrast, *Lague et al.* [2005] modeled mean daily discharge following *Crave and Davy* [2001], and defined the

pdf of discharge normalized by the mean daily discharge ($Q/Q_b = Q^*$) as

$$pdf(Q^*) = \frac{k^{k+1}}{\Gamma(k+1)} \exp\left(-\frac{k}{Q^*}\right) Q^{*-(2+k)}, \quad (11)$$

where Γ is the gamma function, and k is a variability parameter that varies from 0.1 (high variability) to 3 (low variability). Equation (11) is an inverse gamma distribution with a scale parameter k and shape parameter $(k + 1)$ [*Evans et al.*, 2000]. Essentially, the inverse gamma distribution combines an exponential tail for low discharges with a power law distribution of large floods, where the tail of large events is heavy relative to an exponential distribution (Figure 1b). To avoid binning issues when comparing actual discharge data (section 3.2), we plot the complementary cumulative distribution function (*ccdf*) instead of equation (11), which is defined as

$$ccdf(Q^*) = \Gamma(k/Q^*, k+1), \quad (12)$$

where $\Gamma(a,x)$ is the regularized gamma function

$$\Gamma(a,x) = \frac{1}{\Gamma(a)} \int_0^x y^{a-1} e^{-y} dy. \quad (13)$$

While the Poisson pulse model used by *Tucker and Bras* [2000] and *Tucker* [2004] has been shown to match rainfall data well using independent exponential distributions of storm interval, duration, and intensity, the conversion from rainfall to discharge is of course more complex than represented in the simplified hydrologic model used by *Tucker and Bras* [2000]; adequately modeling runoff distributions based on rainfall distributions requires more sophisticated treatment of catchment-scale infiltration, evapo-transpiration, soil moisture response, nonlinear runoff processes, and flood routing through the channel network. Alternatively, stream gage records can be studied directly. *Turcotte and Greene* [1993] suggested that peak flow distributions follow a power law scaling, where the ratio of the ten-year peak discharge to the one-year peak discharge defines a variability factor that depends on climate. *Malamud and Turcotte* [2006] tested the predictions of a power law flood scaling and found good agreement with paleo-flood records on the Colorado River in the Grand Canyon. *Molnar et al.* [2006] expanded on the analysis of *Turcotte and Greene* [1993] to incorporate gaging stations across the United States, and analyzed both peak flow records and records of mean daily discharge, finding that both sets of records tend to have power law tails for the range of climate zones and catchment sizes tested. Indeed, only 3% of the 144 gaging stations analyzed by *Molnar et al.* [2006] exhibited exponential tails. *Lague et al.* [2005] also defined the slope of the power law tail, expressed as $2 + k$ in equation (11), as a climate variability factor analogous to that developed by *Turcotte and Greene* [1993]. Following these studies, we assume that equation (11) is broadly applicable for upland catchments, as supported by our own analyses of discharge records in the San Gabriel Mountains (section 3.2). Although not intuitively obvious, the difference between an exponential and power law tail to the discharge probability distribution significantly influences the predicted relation between channel steepness and erosion rate, as developed by *Tucker* [2004] (exponential tail) and *Lague et al.* [2005] (power law tail) and illustrated below.

3. Application: San Gabriel Mountains

[13] We use the San Gabriel Mountains of California to evaluate the controls on steady state channel steepness using (1) an extensive data set of catchment-averaged cosmogenic radionuclide (CRN) derived erosion rates [*DiBiase et al.*, 2010] (section 3.1), (2) an analysis of long time series of hydrologic data (section 3.2), and (3) detailed field observations of channel morphology and bed state (section 3.3).

3.1. Prior Work

[14] The San Gabriel Mountains (SGM) lie along a large restraining bend in the San Andreas Fault, just north of Los Angeles, California (Figure 2). A series of north-dipping thrust faults along the southern range front accommodates most of the convergence, and sets up a strong W-E gradient in uplift rate and topographic relief [*Spotila et al.*, 2002]. Additionally, this gradient in uplift rate has been sustained long enough such that we can investigate a number of moderately sized ($\sim$1–100 km^2) catchments developed in similar lithologies and experiencing similar climate forcing that have adjusted to differing rates of relative base level fall. *DiBiase et al.* [2010] measured in situ produced cosmogenic ^{10}Be concentrations in active stream sands from 50 basins spanning the range to quantify millennial erosion rates ranging from 35 to 1100 m/Ma (Figure 2). The basins range in size from 0.1 to 175 km^2, and were chosen to sample a wide range of relief. For each basin larger than 3 km^2, a representative channel steepness index was determined from freely available 10 m resolution digital elevation models following the methodology of *Ouimet et al.* [2009] and *Wobus et al.* [2006a]. Channel steepness ranges from 30 to 180 m$^{0.9}$, and increases monotonically with erosion rate [*DiBiase et al.*, 2010]. Mean annual precipitation (MAP) varies with elevation from 500 mm/yr in the Los Angeles basin to over 1000 mm/yr along the range crest, and decreases again to 200 mm/yr in the rain shadow to the north; MAP in sampled catchments spans a range of 600–1000 mm/yr. The range lithology is composed mainly of crystalline basement rocks and Mesozoic granitic intrusions, and rock type appears to play a minor role, with no measureable difference between end-member cases of anorthosite, schist, and granite expressed in the k_s-E relationship [*DiBiase et al.*, 2010].

3.2. Climate and Discharge Records

[15] Streamflow in the San Gabriel Mountains has historically been heavily monitored. While only two basins are actively gaged by the USGS at present (Arroyo Seco and Big Rock Creek), twentieth century records for dozens more can be easily obtained. For this study, we selected 9 gages that have records spanning at least 40 years, and have minimal anthropogenic impact (e.g., dams, diversions) (Table 1). Mean daily discharge scales linearly with drainage area across 3 orders of magnitude, corresponding to a mean annual runoff of $\sim$280 mm/yr, about 30% of

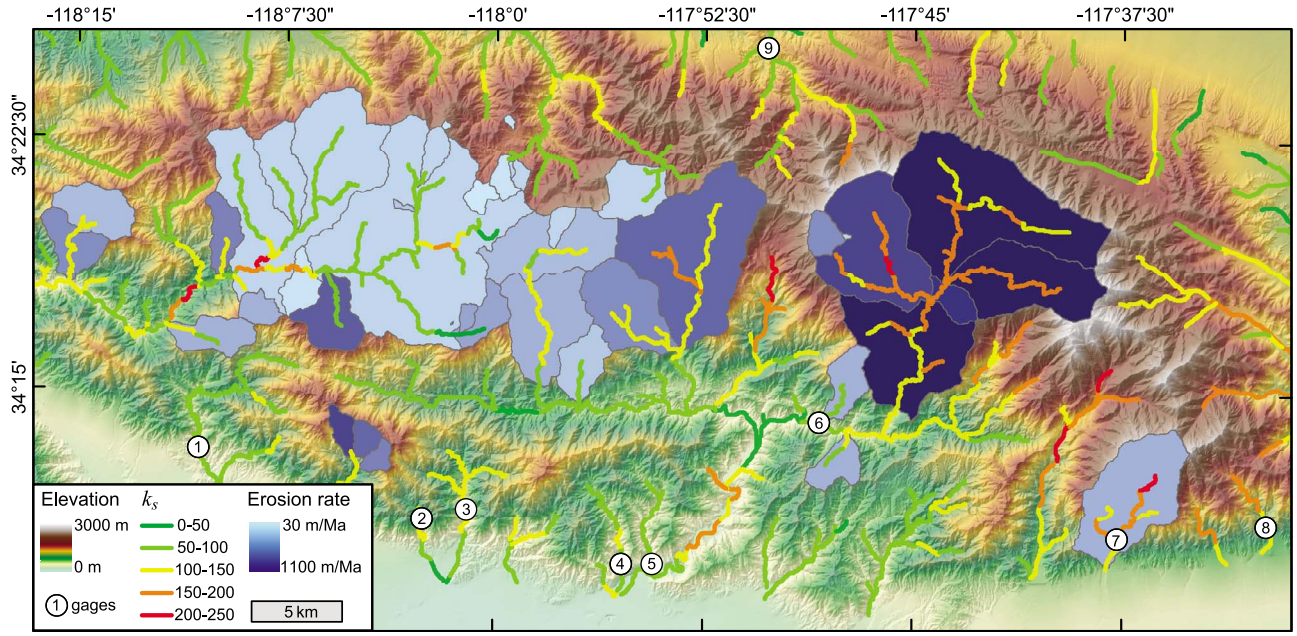

Figure 2. Map of San Gabriel Mountains, California, showing elevation over shaded relief. Catchments with detrital CRN erosion rates measured by *DiBiase et al.* [2010] highlighted in blue according to erosion rate. The stream network (drainage area >2 km^2) is color coded by channel steepness index, which increases with erosion rate from west to east. USGS stream gages listed in Table 1 are shown by numbered circles.

average rainfall as expected for losses to infiltration and evapotranspiration (Figure 3).

[16] To test the applicability of the inverse gamma distribution (equations (11)–(12)) [*Crave and Davy*, 2001; *Lague et al.*, 2005], we normalized flows by the mean of all daily flows for each respective gage, and generated a rank-frequency plot of all values (equivalent to the *ccdf*) [*Newman*, 2005]. Equation (12) fits the SGM discharge data well using a variability factor $k \sim 0.4$–0.6 (Figure 4), much better than the best fit exponential distribution, but not perfectly. As shown in Figure 4, there is a slight separation between two groups of gages; small catchments along the southern range front appear to experience slightly more frequent moderate floods ($10 < Q^* < 100$). We emphasize that while the inverse gamma distribution, with only one free parameter (k), cannot capture such subtle differences between individual gages, most of the discharge data lie within $k = 0.5 \pm 0.1$, and we make the assumption that flood distributions across the SGM are similar and adequately described by this range of k. For comparison with the approach of *Tucker* [2004], we also used hourly rainfall station data in the SGM to calibrate the Poisson pulse model of *Eagleson* [1978] similar to *DiBiase et al.* [2010]. We assume spatially uniform Horton overland flow, and scale mean runoff to equal 280 mm/yr for direct comparison to discharge data. Specific model parameters are given in Table 2.

3.3. Channel Width and Sediment Cover Surveys

[17] We conducted field surveys of over 40 km of river channels to produce an extensive data set detailing the distribution of channel width and sediment cover across the range. Many, but not all of these reaches lie within basins sampled for detrital CRN-derived erosion rates. For the context of this paper, we focus on channel segments that can be considered equilibrated; that is, the long profile lacks prominent knickpoints in or above the surveyed section, and the upstream extent of the drainage network can be fit with a single channel steepness index and concavity [*Wobus et al.*,

Table 1. USGS Stream Gages Used in This Study

Name	Site Number	Latitude	Longitude	Area (km^2)	Q_b (m^3/s)	R_b (mm/yr)	Record Length
(1) Arroyo Seco	11098000	34.222	−118.177	41.4	0.28	214	1910–2011
(2) Little Santa Anita Creek	11100500	34.187	−118.043	4.8	0.03	179	1916–1979
(3) Santa Anita Creek	11100000	34.192	−118.016	25.1	0.19	238	1916–1970
(4) Fish Creek	11084500	34.166	−117.923	16.5	0.13	252	1916–1979
(5) Rogers Creek	11084000	34.165	−117.906	17.2	0.08	148	1917–1962
(6) E.F. San Gabriel River	11080500	34.236	−117.805	219.1	2.01	290	1932–1979
(7) Cucamonga Creek	11073470	34.179	−117.628	25.1	0.23	284	1929–1975
(8) Day Creek	11067000	34.185	−117.539	11.8	0.12	315	1928–1972
(9) Big Rock Creek	10263500	34.421	−117.839	59.3	0.50	265	1923–2011

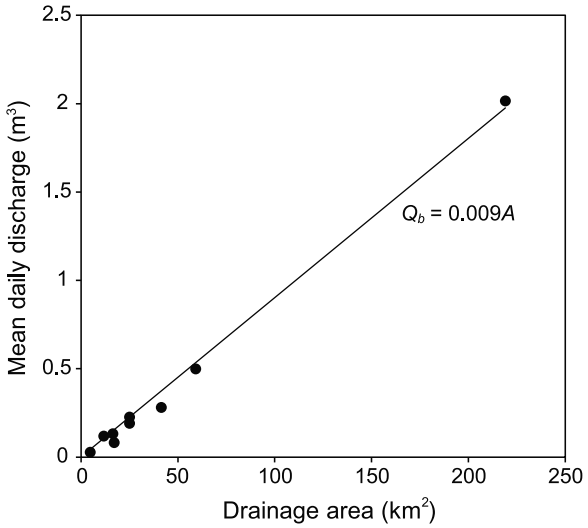

Figure 3. Mean daily discharge plotted against drainage area for USGS stream gages listed in Table 1, with linear least squares fit forced through origin.

2006a]. We characterize channel segments as either low relief (k_s = 30–100) or high relief (k_s = 100–180).

[18] For each of our field surveys, we used a laser rangefinder and electronic data logger to record measurements of bankfull channel width and percent exposed bedrock (estimated visually to the nearest 10%) in the channel bed at intervals of approximately 20–40 m, over channel lengths ranging from 700 m to 4 km. We measured channel width using a laser rangefinder, based on vegetation lines and slope breaks in channel cross sections. We supplemented our surveys with point measurements of channel width taken along streams we did not survey in detail. In order to avoid biasing width measurements toward the high-resolution surveys, we averaged the logarithm of width and drainage area between major tributary junctions for each survey.

Table 2. Model Parameters Used for Fit to SGM Erosion Rate Data

Parameter	Value	Units
k_e	4.3×10^{-12}	$m^{2.5}\ s^{2}\ kg^{-1.5}$
τ_c	45	Pa
k_q	9×10^{-9}	$m\ s^{-1}$
k_w	15	$m^{-0.65}\ s^{0.55}$
k_t	1000	$m^{-7/3}\ s^{-4/3}\ kg$
k	0.5	dimensionless
ω_s	0.25	dimensionless
ω_b	0.55	dimensionless
a	3/2	dimensionless
α	2/3	dimensionless
β	2/3	dimensionless
P[a]	9.94	m/yr
T_r[a]	7	h
T_b[a]	238	h

[a]Poisson pulse rainfall parameters [*Tucker*, 2004].

Figure 5 shows the results of our width measurements plotted against upstream drainage area. The widths of both high and low relief channel reaches follow similar scaling with drainage area, and furthermore lie on the same general trend as a world-wide compilation of similar data for bedrock channels [*Whipple*, 2004; *Wohl and David*, 2008]. While some authors argue for channel narrowing as a means to increase erosional efficiency in steep landscapes [*Duvall et al.*, 2004; *Whittaker et al.*, 2007; *Yanites and Tucker*, 2010], this appears to not be the case for graded streams in the San Gabriel Mountains, consistent with earlier findings in the King Range, CA [*Snyder et al.*, 2003a]. As discussed by *Whipple* [2004] and consistent with analysis by *Yanites and Tucker* [2010] and observations by *Whittaker et al.* [2007], channel width response is likely strongest during transient adjustment and where rock uplift is localized along a downstream segment of a river profile [e.g., *Lavé and Avouac*, 2001]. Thus we can rule out channel width as a cause for increasing erosional efficiency with relief for

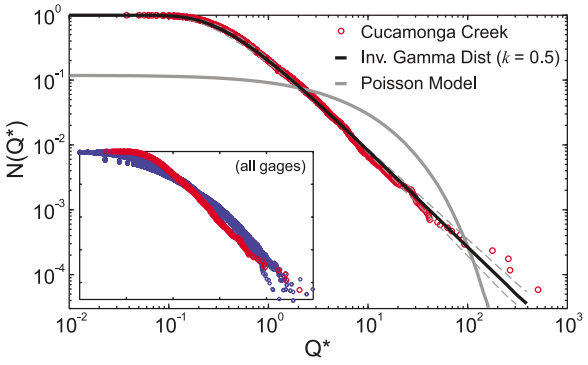

Figure 4. Plot of exceedence frequency as a function of non-dimensional daily discharge ($Q^* = Q/Q_b$) for Cucamonga Creek gage, showing inverse gamma distribution with k = 0.5. Gray dashed lines show inverse gamma distribution with k = 0.4 and k = 0.6. Poisson model in gray is generated using parameters calibrated from rainfall station data at Mt. Baldy (Table 2). Inset shows Cucamonga Creek discharge distribution (red) in comparison to other gages in Table 1 (blue).

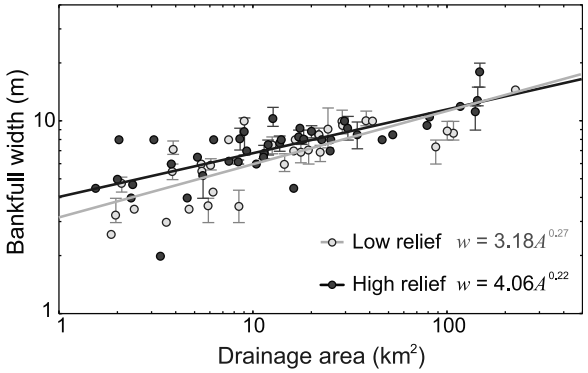

Figure 5. Bankfull channel width plotted against drainage area for SGM channels, showing the similarity of power law fits through low relief (k_s < 100) and high relief ($k_s \geq$ 100) channels. For channels surveyed in detail, we show the log-averaged value of widths measured between major tributary junctions (typically 5–50 measurements), with error bars indicating the inner quartile range. No error bars are shown for individual width measurements (those not associated with detailed surveys).

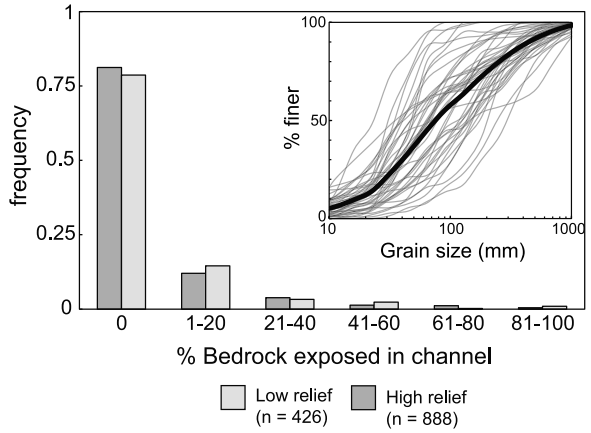

Figure 6. Histogram of bedrock exposure measured in surveys of SGM channels comparing low relief ($k_s < 100$) and high relief ($k_s \geq 100$) channels. Inset plot shows grain size distributions for 44 pebble counts across the range (gray lines), with D_{50} values ranging from ~22–180 mm. Black line indicates the grain size distribution of all pebble count data taken together.

steady state channels in the San Gabriel Mountains, and possibly in general.

[19] At each survey point, we also estimated the percent of exposed bedrock on the channel bed. As shown in Figure 6, bare bedrock channels are rare in the San Gabriel Mountains, and the mean of all reaches, both high and low uplift, is ~4% exposure. Most importantly, while our observations of bed conditions at low flow are unlikely to reflect conditions during floods, we see no trend in percent bed exposure across the range. Additionally, many range front channels grade smoothly into fan deposits, suggesting that the shear stress exponent for detachment-limited incision is similar to that of transport-limited rivers ($n \sim 1$ for bed load transport [*Meyer-Peter and Müller*, 1948]). Moreover, as shown by *Whipple and Tucker* [2002], if the shear stress exponent for detachment-limited incision is greater than that for bed load transport ($n > 1$), channels must become increasingly buried in sediment as relief and erosion rate increase, a process that will tend to force channels into a transport-limited condition in which $n \sim 1$ pertains. While *Whipple and Tucker* [2002] used an effective discharge model (e.g., equation (9)) to develop this argument, it is equally applicable to the stochastic-threshold models used in this study, provided that the threshold for motion is equal to that of incision [e.g., *Sklar and Dietrich*, 2004]. Because our observations do not support an increase in the degree of bed cover with erosion rate, we rule out nonlinear bedrock incision processes ($n > 1$) as a means of increasing erosional efficiency as relief increases in the San Gabriel Mountains.

[20] Last, while we did not quantify the threshold shear stress in the SGM directly, we can use a Shields criterion to approximate a minimum required shear stress based on that needed to mobilize the alluvial bed material,

$$\tau_c = 0.03(\rho_s - \rho_w)D_{50}, \tag{14}$$

where 0.03 is a conservative estimate of the critical Shields stress for initiation of motion in mixed grain-size beds [*Buffington and Montgomery*, 1997], D_{50} is the median grain size, and ρ_s and ρ_w are sediment (~2700 kg/m^3) and water (1000 kg/m^3) densities, respectively. We conducted pebble counts of bed surface material at 44 locations across the SGM, consisting of ~100 grains each. Additionally, we estimated median grain size by eye along each of our channel surveys, with periodic calibration by more detailed point counts. We find that at the reach scale (ca. 100 m), D_{50} varies widely, from 22 to 180 mm (Figure 6, inset, gray lines). There is no systematic variation with relief. For simplicity, we assume a D_{50} of 90 mm, corresponding to τ_c = 45 Pa, based on the median of all point counts combined (Figure 6, inset, black line), and consistent with the median of all estimated values from channel surveys (not shown).

3.4. Comparing Model Predictions and Data in the SGM

[21] Using the above field observations and discharge records as constraints, we tuned the model of *Lague et al.* [2005] (combination of equations (8), (10), and (11)) to fit the relationship between channel steepness and erosion rate quantified in the SGM by *DiBiase et al.* [2010]. While *Tucker* [2004] and *Lague et al.* [2005] provided analytical solutions to end-member cases for exponential and inverse gamma flood distributions, respectively, we opted to numerically integrate equation (10) using an adaptive Simpson's method [*Gander and Gautschi*, 2000] in all our analyses to smoothly capture the full range of model behavior. We used a generalized Darcy-Weisbach friction relation ($\alpha = \beta = 2/3$; $k_t = \rho_w g^{2/3} C_f^{1/3}$) with non-dimensional friction coefficient $C_f = 0.01$, following *Tucker* [2004]. As mentioned above, we find no evidence that the degree of rock exposure varies with channel steepness or erosion rate in steady state channels in the SGM, so we make the assumption that the shear stress exponent is equal to that of common bed load transport formulae [e.g., *Meyer-Peter and Müller*, 1948], giving $n = a\beta = 1$ in equation (8).

[22] Assumptions regarding channel width scaling are somewhat more complicated. In order to equate the channel steepness index measured from field data (reference concavity = 0.45) with that in equation (8), we must fix the ratio m/n to 0.45, which implies a width-discharge exponent value of 0.55 (ω_b in equation (4a)). The regressed value of ω_b from SGM channels is much lower (Figure 5), so for internal consistency here we determine k_w by regressing the width data in the SGM using a fixed value of $\omega_b = 0.55$. Although a bit awkward and suggestive that the controls on channel profile concavity in the SGM are not fully understood [*Snyder et al.*, 2003a], these adjustments have little impact because the width scaling holds constant across the landscape (Figure 5). Only a systematic change in width-area scaling with channel steepness will influence the shape of the k_s-E relationship. We fix ω_s to 0.25, based on general results from a 2D cross-sectional flow model as mentioned earlier (auxiliary material; Figures S1 and S2 in Text S1). As noted earlier, mean runoff and discharge variability (R_b = 280 mm/yr; $k = 0.5 \pm 0.1$) are calibrated against USGS gaging records, and we use field estimates of D_{50} to determine a value of 45 Pa for τ_c.

[23] Given these constraints, there is only one free parameter, k_e, a measure of rock strength, which we tune to fit the model to our data, minimizing the RMS error in erosion rate

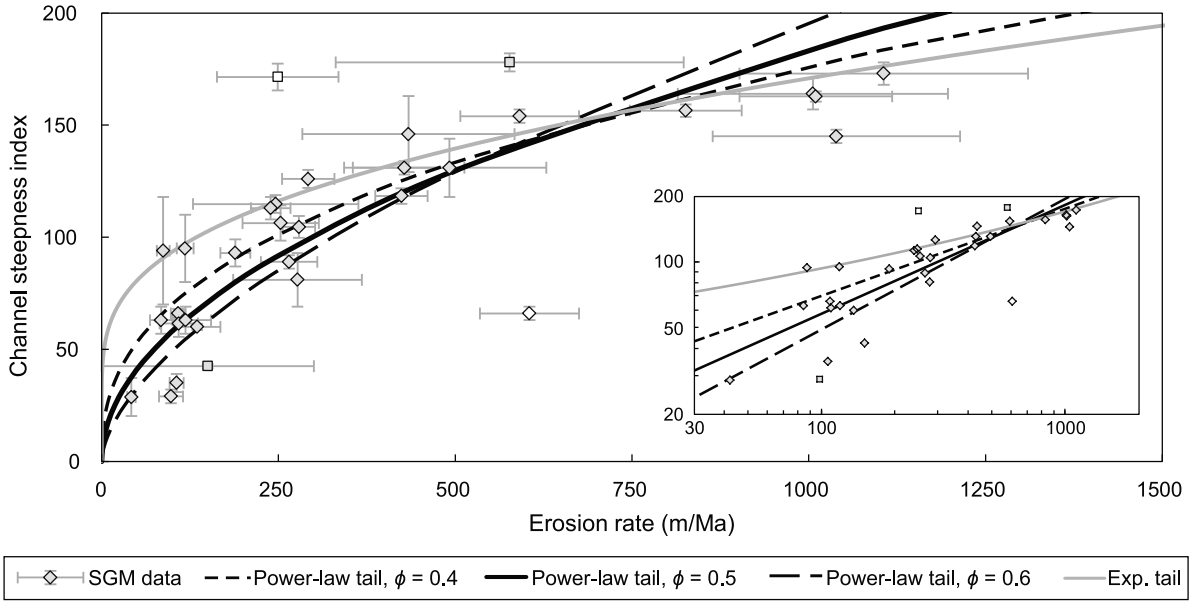

Figure 7. Plot of channel steepness index against catchment-average erosion rate for the San Gabriel Mountains (gray and hollow symbols). Erosion rates are derived from ^{10}Be concentrations in stream sands measured by *DiBiase et al.* [2010], with error bars showing 1σ analytical uncertainty in erosion rate and uncertainty in k_s as described by *DiBiase et al.* [2010]. Black line shows best fit of equation (10) through erosion rate data using the inverse gamma distribution (equation (11); parameters given in Table 2). Dashed lines show fits reflecting range of plausible ϕ values. Gray line shows similar fit using an exponential discharge distribution [e.g., *Tucker*, 2004]. Hollow symbols indicate two outliers not included in fit calculation. Square symbols indicate repeat measurements from *DiBiase et al.* [2010] that have been combined into single points.

for each of our CRN data points (black line, Figure 7). We also show two fits (dashed lines, Figure 7) reflecting the range of uncertainty in k (0.4–0.6) and the quantity $\alpha(1-\omega_s)$ (0.45–0.55, Figure S2 in Text S1). To highlight the influence of the choice of *pdf(Q)* in equation (10), we also fit the *Tucker* [2004] model to the SGM data using a similar approach (gray line, Figure 7). We use Poisson rainfall parameters as described above, and hold all other parameters equal to the *Lague et al.* [2005] case except for k_e, which we again vary to minimize RMS error in erosion rate. While both the *Tucker* [2004] and the *Lague et al.* [2005] model capture the rollover of the k_s-E relationship at high erosion rates, the *Tucker* [2004] model deviates from a power law at low erosion rates, precisely where the influence of an erosion threshold is most important (Figure 7, inset).

3.5. Discussion of Model Application to the SGM

[24] Whereas the *Lague et al.* [2005] model explains much of the variability in the SGM data, there are two notable deviations. Channels with $k_s < 40$ erode more rapidly than predicted by the model, which by definition assumes that hillslope erosion is set by the channel incision rate (i.e., steady state) and thus that erosion rate goes to zero for $k_s = 0$. One plausible explanaton is that these slowly eroding, low-relief catchments are not in steady state, but rather in a state of slowly declining relief. Under such a scenario it would be likely that catchment-mean erosion rate would exceed the channel incision rate: hillslope erosion will continue as long as some local relief persists even where channel incision has ceased. A second misfit is noted in that rapidly eroding catchments ($E > 500$ m/Ma) tend to be less steep than predicted (Figure 7). Potential reasons for this misfit include an increased influence of debris flows in the high relief landscapes of the SGM, inaccuracies of the detrital CRN method at high erosion rates, changes in bed roughness, or differences in the flood frequency probability distribution not resolved by equation (11).

[25] The *Tucker* [2004] model appears to better capture the behavior of rapidly eroding catchments, but at the cost of significant misfit at low erosion rates due to the thinner tail of the exponential flood distribution. Whereas the considerable scatter in the SGM erosion rate data prevents discriminating between the *Tucker* [2004] and *Lague et al.* [2005] models, we note that the power law tail exhibited by SGM discharge data strongly supports the *Lague et al.* [2005] model. Indeed, it is at low erosion rates where differences in the tail of the flood distribution becomes most important, as the critical flow needed to overcome the erosion threshold, Q_c, increases with decreasing channel steepness because deeper flows are required to exceed the threshold shear stress in channels with gentler slopes. It is therefore quite satisfying that the model that includes the fatter power law tail to the flood distribution fits the data at low to moderate channel steepness considerably better (Figure 7). The ability of this simple model, which includes no treatment of bed cover and dynamic width adjustment, to explain the shape of the k_s-E relationship reinforces our field observations that indicate that these factors are not important in the SGM.

[26] We speculate, but cannot yet definitively demonstrate, that this finding has general implications and is not

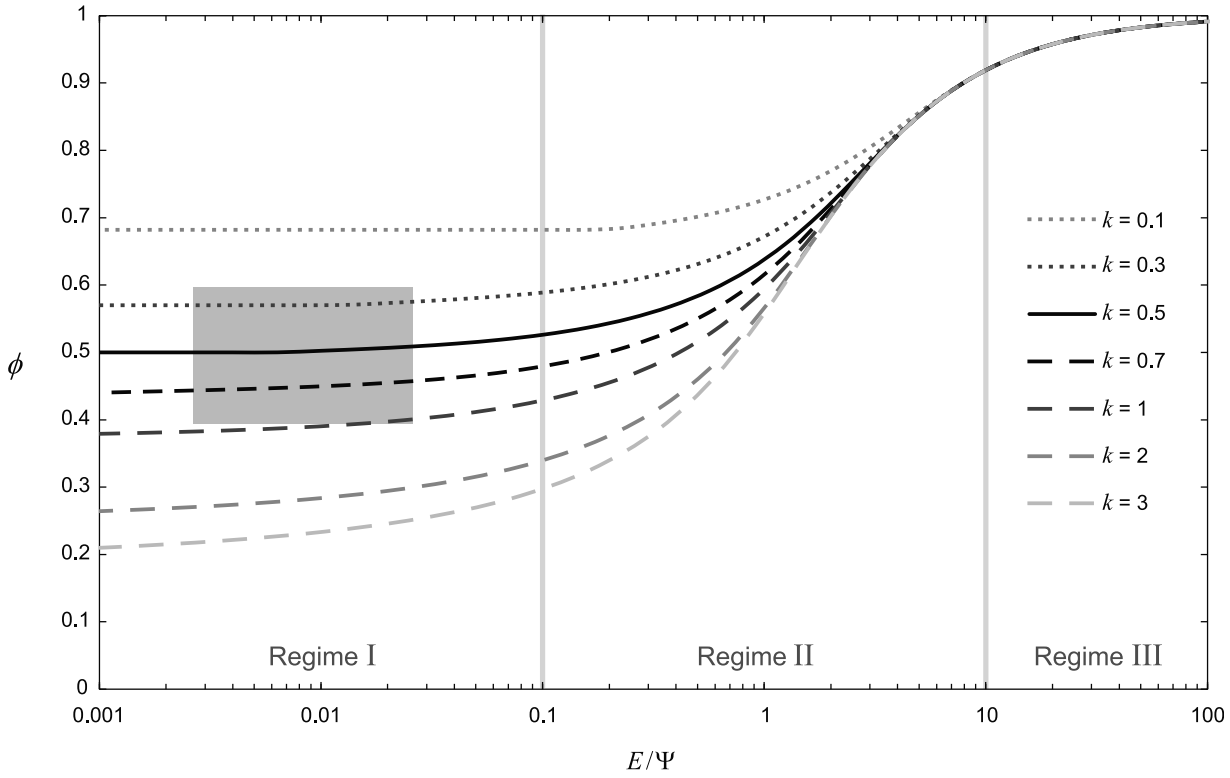

Figure 8. Plot of power law exponent from equation (1) against erosion rate normalized by the threshold term Ψ from equation (7), assuming a constant threshold shear stress (τ_c = 45 Pa). Vertical gray bars separate 3 regimes described by *Lague et al.* [2005]. Regime I (low E/Ψ) is dominated by the threshold term, and the shape of the k_s-E relationship (dictated by ϕ) is controlled by the at-a-station shear stress-discharge exponent, $\alpha(1 - \omega_s)$, and discharge variability (k, equation (11)). Regime III (high E/Ψ) approaches the effective discharge approximation (equation (8)), where ϕ is set by the exponent n in the instantaneous incision rule (equation (7)). We use n = 1 in all calculations. Regime II is transitional. Gray box shows conditions in the SGM, indicating the range of erosion rates and uncertainty in discharge variability.

unique to the SGM; that under steady state conditions and uniform rock uplift rate in general, the effects of bed cover variations and dynamic width adjustment tend to be negligible compared to the effects of a probability distribution of floods acting in the presence of significant detachment or mobilization thresholds. If true, this implies that much can be learned about the relationships among climate, topography and erosion rate from further study of the behavior of the stochastic-threshold model of *Lague et al.* [2005], which we undertake in the following section.

4. Application: Climatic Controls on the Relief-Erosion Rate Relationship

4.1. General Model Behavior

[27] The relationship between steady state erosion rate and relief (as quantified by the channel steepness index, k_s) is both a critical input for landscape evolution and coupled climate-landscape-tectonics models, and directly measureable. With the widespread availability of digital elevation models, and an increasing number of studies quantifying catchment-averaged erosion rates using cosmogenic radionuclides, we are able to begin untangling the first-order effects of topography, climate, and rock strength in controlling bedrock incision rate. In the previous section, we showed that a nonlinear ($\phi \sim 0.5$; equation (1)) relationship between erosion rate and channel steepness in the San Gabriel Mountains could be explained well using the stochastic-threshold model of *Lague et al.* [2005]. Other regions with similar data suggest that ϕ ranges from 0.25 to 1 [*Kirby and Whipple*, 2001; *Ouimet et al.*, 2009; *Snyder et al.*, 2003b; *Wobus et al.*, 2006a]. In this section, we will summarize some of the key points of *Lague et al.* [2005] within the context provided by the San Gabriel Mountains example. We focus here on the controls on the shape of the relationship between channel steepness and erosion rate, differences that are most clearly manifest by the power law exponent (ϕ) of equation (1). The power law form of the predicted relationship is directly a result of combing a power law relationship between I and Q^* (equation (8)) with a power law distribution of floods (equation (11)). Following a discussion of the controls on the power law exponent (ϕ), we explore how changing climate mean and variability influence the relationship between channel steepness and erosion rate.

[28] A convenient way to show the variations in the relationship between channel steepness and erosion rate is to plot the power law exponent, ϕ, against erosion rate normalized by the threshold term Ψ (Figure 8). As discussed by *Lague et al.* [2005], there are 3 regimes expressed in Figure 8, depending on the relative importance of the

threshold parameter Ψ (or equivalently, the return time of the critical discharge, Q_c^*). At high incision rate (or negligible threshold, Regime III), the relation approaches the approximation of equation (9), and k_s is proportional to $E^{1/n}$ (equation 1 with $\phi = 1/n$), where n is expected to reflect process mechanics [*Whipple et al.*, 2000], for any flood distribution. On the other hand, when the threshold is large compared to the incision rate (Regime I), the exponent ϕ in equation (1) is independent of n (or a in equation (2) and thus erosion process mechanics), and rather depends primarily on k (discharge variability) and the at-a-station shear stress-discharge exponent, $\alpha(1 - \omega_s)$, in equation (5)) according to the following relation [*Lague et al.*, 2005]:

$$\phi = \frac{\alpha(1-\omega_s)}{\beta(1+k)}. \tag{15}$$

where β is from the flow resistance relationship and takes values of 7/10 for the Manning relation and 2/3 for the generalized Darcy-Weisbach relation (equation (3)). Between the end-member cases of Regime I and III lies a transitional zone (Regime II). The San Gabriel Mountains lie entirely within the threshold-dominated regime (Figure 8). An alternative indicator of the dominant regime is the return time of the critical flow which can be estimated using equation (5) of *Lague et al.* [2005]. In the SGM, it ranges from 500 days (low relief) to 50 days (high relief), indicating a dominance of threshold effects. Thus uncertainty in most parameters (especially τ_c) can be subsumed into the high uncertainty in k_e, which we varied to fit the model to the SGM data. The predicted ϕ of 0.5 for the SGM (from equation (15)) matches well with a simple error-weighted least squares power law fit to the erosion rate data, which results in a fitted exponent of 0.48 (95% confidence range = 0.36–0.75; $R^2 = 0.64$).

[29] We use this well-constrained case to fix all parameters except mean runoff (k_q) and climate variability (k) to explore the role of climate alone in controlling incision rates. Figure 9a shows the effect of changing mean runoff (R_b) by an order of magnitude in either direction from the SGM case. As R_b does not factor into ϕ or Ψ, the shape of the k_s-E relationship stays the same; however, increasing mean runoff increases erosion rate for a given channel steepness and decreasing mean runoff does the opposite [*Lague et al.*, 2005]. It should also be noted that the influence of changing mean runoff is partially offset by corresponding changes in channel width (i.e., equation (4a)). Changing climate variability (k) induces a more complex response. As shown in Figure 9b, the power law exponent in the k_s-E relationship (ϕ) decreases with decreasing variability (large k). Thus the k_s-E relationship becomes increasingly nonlinear as discharge variability decreases (large k, Figure 9b). Additionally, when in the threshold-dominated regime, increasing climate variability, while holding all else equal, increases erosion rate for a given k_s, (Figure 9b). The opposite is true for channels in regime III [*Lague et al.*, 2005].

4.2. Co-variation of Mean Runoff and Climate Variability

[30] The above analysis indicates that all else equal, wetter and more variable climates increase erosional efficiency, while dry and steady climates are less efficient, a fairly intuitive result and one familiar from previous work [*Lague et al.*, 2005; *Tucker*, 2004]. A more challenging question, and one often postulated by workers interested in global climate change and climate/tectonics feedbacks, is whether dry and variable climates can be more efficient than stable, wet climates [*Molnar*, 2001; *Molnar et al.*, 2006; *Zhang et al.*, 2001]. While *Istanbulluoglu and Bras* [2006] explicitly modeled the catchment-scale response of soil moisture and vegetation cover to changes in rainfall intensity, such field data are scarce, and we focus instead on exploring only the observed relationships between mean runoff and variability from gaged streams. *Turcotte and Greene* [1993] argued that discharge variability was highest in arid environments, and lowest in humid environments. *Molnar et al.* [2006] extended this analysis and found that, at least for gages within the United States, there is a roughly inverse relationship, albeit with much scatter, between mean annual runoff and variability expressed by k ($R_b \sim k^{1.6}$). Using precipitation records compiled by *Hawk* [1992], *Tucker* [2004] and *Istanbulluoglu and Bras* [2006] found a similar relationship between a metric of storm variability and mean annual precipitation across the United States.

[31] Here we extend the analyses of *Lague et al.* [2005] and *Molnar et al.* [2006] to explore quantitatively the competition between the influence of mean runoff and variability on channel incision when the two are inversely related according to the relationship

$$k = \left(\frac{R_b}{B}\right)^C, \tag{16}$$

where B and C are empirically derived constants [*Molnar et al.*, 2006]. B and C values of 850 mm/yr and 0.625, respectively, describe the central tendency in the discharge data compiled by *Molnar et al.* [2006], but we emphasize that there is significant scatter in the data (B ranges from ~20–1000; C ranges from ~0.5–1.0), which in addition covers only the continental United States and does not apply across all climate zones. Indeed some tropical climates, where heavy rainfall is dominated by tropical cyclones, can be both wet and variable (e.g., Taiwan [*Lague et al.*, 2005]).

[32] Figure 9c shows the effect of varying mean annual runoff from 0.03 to 2.8 m (corresponding to a range in k from 0.12 to 2.1 using equation (16) with the B and C values given above), while holding all other parameters equal to the SGM case. The crossing of curves at low erosion rates (<200 m/Ma) represents a transition in climate sensitivity; low-steepness channels are more sensitive to changes in climate variability than mean runoff, while the opposite is true for steep channels (see also Figures 9 and 10). Channels with low steepness require larger floods to overcome thresholds of erosion: floods that can actually be more common in dry, but variable environments (see Figure 6 of *Molnar et al.* [2006]).

[33] Plotting erosion rate against mean runoff highlights this behavior. Figure 10a shows the relationship between erosion rate and mean runoff for a range of channel steepness index values, using the parameters in Table 2 and values for B and C given above. For channels with low channel steepness ($k_s < 100$), there is a hump in the erosion-runoff relationship between mean runoff (R_b) of 100 and 400 mm/yr, indicated by the white diamonds. For channels

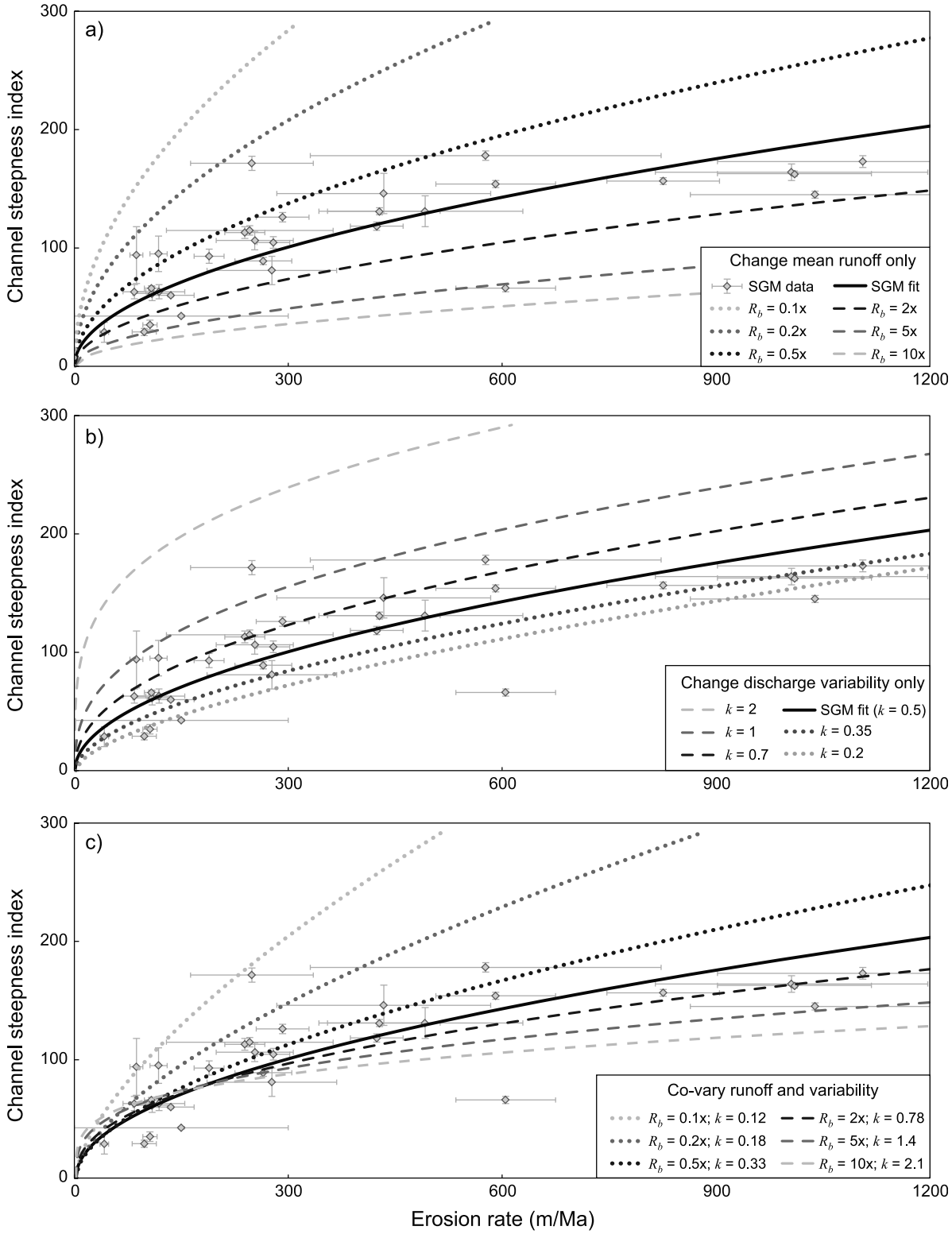

Figure 9. Plot of channel steepness index against erosion rate showing the influence of (a) changing mean runoff only, (b) changing discharge variability only, and (c) co-varying mean runoff and discharge variability according to the relationship given by equation (16). Gray symbols and black line indicate SGM data and fit from Figure 7 (R_b = 280 mm/yr; k = 0.5).

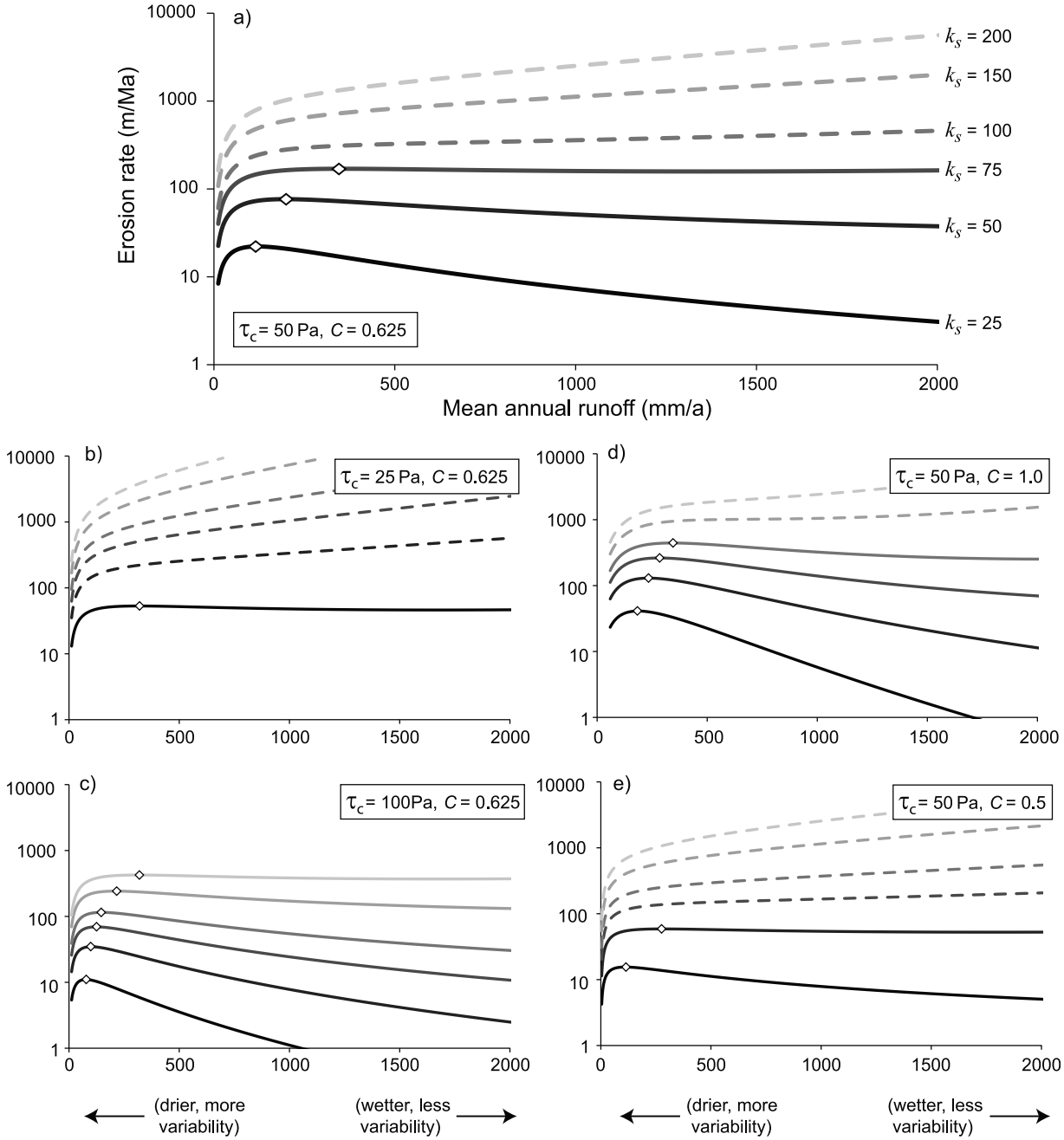

Figure 10. Plot of erosion rate versus mean runoff as a function of channel steepness index when discharge variability and mean runoff vary according to equation (16). Solid lines and diamonds indicate the presence and location of a peak erosional efficiency, while dashed lines indicate a monotonic relationship between erosion rate and mean runoff. A peak in erosional efficiency is enhanced by decreasing channel steepness (Figures 10a–10e), increasing erosion threshold magnitude (Figure 10c), or strengthening the relationship between mean runoff and discharge variability (Figure 10d).

with high channel steepness ($k_s \geq 100$) the relationship between erosion and runoff is monotonic (dashed lines), though there is still a significant flattening of the relationship for $R_b > \sim$200 mm/yr. We emphasize that while this peak in erosional efficiency (erosion rate for a given channel steepness) roughly matches that observed by *Langbein and Schumm* [1958], and predicted by *Istanbulluoglu and Bras* [2006], it arises here solely because of trade-offs between variability and mean runoff in bedrock channel incision, factors not considered in these other works.

[34] The existence and location of a peak erosional efficiency depend not only on the channel steepness index, but also on the magnitude of the threshold, τ_c, and the strength of the runoff-variability relationship (controlled by C in equation (16)), as shown in Figures 10b–10e. Increasing τ_c has a similar effect on the relationship between erosion and runoff as decreasing channel steepness: by increasing

Q_c^*, discharge variability becomes more important, and the peak is enhanced (Figure 10c). Conversely, for small τ_c, large floods are less important, and the peak is diminished (Figure 10b). Changing C varies the strength of the runoff-variability relationship and thus illustrates the uncertainty associated with the scatter in the data. When C is large, variability increases rapidly with decreasing mean runoff, and the peak in erosional efficiency is enhanced (Figure 10d); when C is small, variability and mean runoff are but weakly related and thus the peak is subdued (Figure 10e). Naturally, Figures 9a and 9b illustrate the model behavior when R_b and k are independent.

[35] The results shown in Figure 10 suggest that the relationship between climate and erosion rate is complex, and changes depending on the ratio of channel steepness to the erosion threshold. While *Molnar et al.* [2006] suggested that change to drier, more variable conditions would rarely increase erosion rate, we show here that such a trend is possible over a wide range of conditions (solid lines in Figure 10). Furthermore, there is a range of parameter space where changing climate does not influence erosional efficiency; that is, the competing effects of decreased variability and increased runoff are in balance. We emphasize again that the relationship between mean runoff and discharge variability expressed by equation (16) only applies to a narrow band of potential climate scenarios (those analyzed by *Molnar et al.* [2006] in the continental U.S.). Even so, Figures 9 and 10 highlight both the potential implications of co-variance between R_b and k and the need for careful site selection when trying to quantify the relationship between climate and erosion rate in the field. These results suggest one plausible explanation for the diversity of published relationships summarized by *Riebe et al.* [2001].

5. Discussion

5.1. Implications for Climate-Tectonic Interactions

[36] The finding that the relationship between channel steepness and erosion rate in the SGM is highly nonlinear ($\phi = 0.5$; Figure 7) and the model implication that this may be a common circumstance (Figure 8) carry important implications for the strength of the hypothesized influence of climate on rock uplift rates and deformation patterns in compressional orogens [e.g., *Hilley and Strecker*, 2004; *Whipple*, 2009; *Whipple and Meade*, 2004; *Willett*, 1999]. *Whipple and Meade* [2004] showed that steady state rock uplift rate in a compressional orogen, U, scales with the tectonic accretionary flux (F_a) and coefficient of erosional efficiency (C_e) according to:

$$U \propto F_a^{\frac{p}{p+1}} C_e^{\frac{1}{p+1}} \tag{17a}$$

$$p = 0.8/\phi, \tag{17b}$$

where the 0.8 arises from the product of the channel concavity index ($\sim$0.5) and the inverse of the Hack's law exponent ($\sim$1.7). A value of $\phi = 0.5$, as found for the SGM and the eastern margin of the Tibetan Plateau [*Ouimet et al.*, 2009], implies $U \propto F_a^{0.6} C_e^{0.4}$, the weakest dependence of rock uplift rate on erosional efficiency considered to be within the range of likely conditions by *Whipple and Meade* [2004].

[37] The analyses illustrated in Figures 9 and 10 exacerbate this apparent weakening of theoretical predictions of the strength of the potential influence of precipitation rate on steady state rock uplift. As discussed by *Stolar et al.* [2006], in the standard stream power river incision models (which ignore the threshold-stochastic effects and potential inverse relationship between mean annual runoff and discharge variability emphasized here) the coefficient of erosional efficiency, C, scales approximately with the square root of mean annual runoff. Combined with the above result, this implies that steady state rock uplift rate varies only weakly with mean annual runoff, $U \alpha F_a^{0.6} R_b^{0.2}$. As illustrated in Figure 10, when thresholds of erosion and the potential co-variation of discharge variability and mean annual runoff are considered, the relation between erosional efficiency and mean annual runoff can be much weaker as cautioned by *Whipple and Meade* [2006] and *Whipple* [2009]. Although we can only speculate for now, this could be one reason why clear field evidence for a strong coupling between climate and tectonics has been difficult to find [e.g., *Whipple*, 2009]. That said, model predictions also indicate that the strongest influence of climate on tectonics will likely be found where channels are steep (Figure 10), where flood discharges are highly variable (Figure 8), and where increases in mean annual runoff are not offset by decreases in discharge variability, such as orogens frequently struck by tropical cyclones like the Central Range of Taiwan [*Lague et al.*, 2005]. Moreover, glaciated mountain ranges may be more sensitive to climate changes and tectonics more responsive to glacial erosion [e.g., *Tomkin and Roe*, 2007].

5.2. Limitations and Future Research Needs

[38] Whereas the simple stochastic-threshold incision model described above is consistent with channel steepness (k_s) and erosion rate (E) data in the SGM, suggesting that the presence of erosion thresholds and discharge variability may be primarily responsible for the strong nonlinearity in the k_s-E relationship (equations (1) and (15)), we cannot yet determine whether climatic effects alone provide a full explanation for the steady state channels in the SGM, nor whether they can potentially explain differences in the relief-erosion rate relationships observed in other landscapes. There are few studies in the literature that provide the range of relief and erosion rates necessary to evaluate this possibility, and even fewer that also have long-term discharge records and field observations to constrain the parameters listed in Table 2. Moreover, the use of decadal to centennial hydrologic records must be used to extrapolate climate conditions over the timescale of erosion rate measurements, which must in turn be long enough to incorporate the influence of large events. Finally, the challenge of quantifying rock strength and erosion thresholds directly makes inter-site comparison difficult. However, given careful site selection, the relationships shown in Figures 9 and 10 serve as a set of testable hypotheses that have the potential to illuminate the currently cloudy empirical relationships between climate and erosion rate.

[39] In particular, detecting a climatic control on erosion rate (i.e., determining the dependence of erosional efficiency on mean annual runoff and discharge variability) requires a

suite of field sites in different climate regimes, each covering a range of relief, but having similar lithology. It is only through the lens of topography that we will be able to resolve the role of mean runoff and discharge variability in controlling erosion rate. An exacting test of the *Lague et al.* [2005] model will require data from field sites chosen to explore independently the roles of mean runoff and runoff variability and their dependences on channel steepness. In addition, there is a need to further explore the controls on k_e and its dependence on substrate properties [e.g., *Sklar and Dietrich*, 2001; *Tressler et al.*, 2010]. Though it is unlikely that this simple model captures the full range of behavior in steady state channels, the fit to the SGM data suggests that the first-order implications of this model may apply to many landscapes. Of course, under transient conditions, a broader suite of controls (sediment tools and cover, process mechanics, channel width) will likely emerge [e.g., *Attal et al.*, 2008, 2011; *Valla et al.*, 2010]: it is channel evolution during periods of transience that will provide the most exacting tests of channel incision models. Whether or not these transient effects need to be accounted for, however, depends on the time scale of the geologic problem. For example, in million-year, orogen-scale studies of climate-tectonic interactions, an assumption of quasi-steady state river incision is probably sufficient to develop relationships among climate, rock type, topography, erosion rate, and tectonic style, even when the landscape is changing over long time periods [*Stolar et al.*, 2006; *Whipple and Meade*, 2006]; the stochastic-threshold model may be sufficient for quantitative analyses at these long time scales as discussed above for steady state conditions. Conversely, in studies directed at extracting the tectonic or climatic history of a specific field area recorded in landscape morphology or sedimentary records, an appreciation for the rich behavior in fluvial systems during periods of adjustment to changing climatic or tectonic conditions is paramount, and a simple stochastic-threshold model is likely inadequate [*Attal et al.*, 2008; *Crosby et al.*, 2007; *Gasparini et al.*, 2007; *Valla et al.*, 2010].

6. Conclusions

[40] We have shown here that a nonlinear relationship between channel steepness index and erosion rate in the San Gabriel Mountains, CA can be explained by a simple bedrock incision model that incorporates a stochastic distribution of discharge events coupled with an erosion threshold [*Lague et al.*, 2005], but does not include the complexities of recent modeling efforts regarding dynamic cross-sectional evolution [*Turowski et al.*, 2009; *Wobus et al.*, 2006b] or detailed accounting for sediment tools and cover effects [*Lague*, 2010; *Sklar and Dietrich*, 2004]. We constrained the relationship using field observations of channel geometry and bed state, along with an analysis of discharge records from throughout the range. We found that for graded channels, in the SGM at least, possibly in general, the role of sediment tools and cover, channel width adjustment, and changes in incision process appear to play a subordinate role to the influence of erosion thresholds and discharge variability. We showed explicitly that the choice of discharge distribution strongly influences the modeled relationship between channel steepness and erosion rate, particularly for low channel slopes, where the heaviness of the flood distribution tail strongly controls the frequency of erosive events.

[41] Based on parameters calibrated from the SGM, we evaluated the implications of the *Lague et al.* [2005] model for the relationship between channel steepness and erosion rate. Bedrock channels in the SGM lie well within the "threshold dominated" regime of *Lague et al.* [2005], which surprisingly implies that the shape of the k_s-E relationship is governed by discharge variability k and the at-a-station discharge exponent $\alpha(1 - \omega_s)$ rather than erosion process, as is almost universally assumed. For threshold dominated channels, erosion is enhanced by increasing mean runoff as well as increasing variability. We imposed an empirical relationship between mean runoff and variability to test if dry, variable climates can be more efficient than wet, stable climates. We extended the analysis of *Molnar et al.* [2006] and found that for channels with a high erosion threshold (or alternatively, low steepness) there exists a peak in erosional efficiency that lies near a mean runoff of 200–400 mm/yr, similar to the relationship observed by *Langbein and Schumm* [1958]. Furthermore, for a large range of parameter space (but excluding tropical climates), erosion rate is predicted by this model to be insensitive to increases in runoff above 500 mm/yr, suggesting that any climatic influence on tectonics in unglaciated landscapes may be restricted to subhumid or drier climates and climates where higher mean annual runoff is not offset by a decrease in discharge variability. The relationships among channel steepness index, erosion rate, and climate variables developed here thus form a set of critical, testable hypotheses that should be explored further to elucidate the complex relationships among climate, topography, and erosion rate.

[42] **Acknowledgments.** We would like to thank all those involved with the field surveys, including B. Adams, E. DiMaggio, N. Gasparini, B. Guralnik, M. Jungers, J. McDermott, D. Stolar, and J. Walsh. Thanks to M. Rossi and G. Tucker for valuable discussion and feedback. J. Kean provided assistance with cross-sectional flow modeling. Excellent and thorough reviews by M. Attal, D. Lague, G. Tucker, and J. Turowski greatly improved the manuscript. Funding for this project was provided by the Geomorphology and Land Use Dynamics program at NSF (EAR-0724194 to K.X.W.).

References

Armitage, J. J., R. A. Duller, A. C. Whittaker, and P. A. Allen (2011), Transformation of tectonic and climatic signals from source to sedimentary archive, *Nat. Geosci.*, *4*(4), 231–235, doi:10.1038/ngeo1087.

Attal, M., G. E. Tucker, A. C. Whittaker, P. A. Cowie, and G. P. Roberts (2008), Modeling fluvial incision and transient landscape evolution: Influence of dynamic channel adjustment, *J. Geophys. Res.*, *113*, F03013, doi:10.1029/2007JF000893.

Attal, M., P. A. Cowie, A. C. Whittaker, D. Hobley, G. E. Tucker, and G. P. Roberts (2011), Testing fluvial erosion models using the transient response of bedrock rivers to tectonic forcing in the Apennines, Italy, *J. Geophys. Res.*, *116*, F02005, doi:10.1029/2010JF001875.

Bagnold, R. A. (1977), Bed load transport by natural rivers, *Water Resour. Res.*, *13*(2), 303–312, doi:10.1029/WR013i002p00303.

Buffington, J. M., and D. R. Montgomery (1997), A systematic analysis of eight decades of incipient motion studies, with special reference to gravel-bedded rivers, *Water Resour. Res.*, *33*(8), 1993–2029, doi:10.1029/96WR03190.

Chatanantavet, P., and G. Parker (2008), Experimental study of bedrock channel alluviation under varied sediment supply and hydraulic conditions, *Water Resour. Res.*, *44*, W12446, doi:10.1029/2007WR006581.

Cowie, P. A., A. C. Whittaker, M. Attal, G. Roberts, G. E. Tucker, and A. Ganas (2008), New constraints on sediment-flux-dependent river incision: Implications for extracting tectonic signals from river profiles, *Geology*, *36*(7), 535–538, doi:10.1130/G24681A.1.

Crave, A., and P. Davy (2001), A stochastic "precipiton" model for simulating erosion/sedimentation dynamics, *Comput. Geosci.*, *27*(7), 815–827, doi:10.1016/S0098-3004(00)00167-9.

Crosby, B. T., K. X. Whipple, N. M. Gasparini, and C. W. Wobus (2007), Formation of fluvial hanging valleys: Theory and simulation, *J. Geophys. Res.*, *112*, F03S10, doi:10.1029/2006JF000566.

Cyr, A. J., D. E. Granger, V. Olivetti, and P. Molin (2010), Quantifying rock uplift rates using channel steepness and cosmogenic nuclide-determined erosion rates: Examples from northern and southern Italy, *Lithosphere*, *2*(3), 188–198, doi:10.1130/L96.1.

DiBiase, R. A., K. X. Whipple, A. M. Heimsath, and W. B. Ouimet (2010), Landscape form and millennial erosion rates in the San Gabriel Mountains, CA, *Earth Planet. Sci. Lett.*, *289*(1–2), 134–144, doi:10.1016/j.epsl.2009.10.036.

Duvall, A., E. Kirby, and D. Burbank (2004), Tectonic and lithologic controls on bedrock channel profiles and processes in coastal California, *J. Geophys. Res.*, *109*, F03002, doi:10.1029/2003JF000086.

Eagleson, P. S. (1978), Climate, soil, and vegetation: 2. Distribution of annual precipitation derived from observed storm sequences, *Water Resour. Res.*, *14*(5), 713–721, doi:10.1029/WR014i005p00713.

Evans, M., N. Hastings, and B. Peacock (2000), *Statistical Distributions*, 3rd ed., 221 pp., John Wiley, New York.

Finnegan, N. J., G. Roe, D. R. Montgomery, and B. Hallet (2005), Controls on the channel width of rivers: Implications for modeling fluvial incision of bedrock, *Geology*, *33*(3), 229–232, doi:10.1130/G21171.1.

Finnegan, N. J., L. S. Sklar, and T. K. Fuller (2007), Interplay of sediment supply, river incision, and channel morphology revealed by the transient evolution of an experimental bedrock channel, *J. Geophys. Res.*, *112*, F03S11, doi:10.1029/2006JF000569.

Gander, W., and W. Gautschi (2000), Adaptive quadrature—Revisited, *BIT*, *40*(1), 84–101, doi:10.1023/A:1022318402393.

Gasparini, N. M., K. X. Whipple, and R. L. Bras (2007), Predictions of steady state and transient landscape morphology using sediment-flux-dependent river incision models, *J. Geophys. Res.*, *112*, F03S09, doi:10.1029/2006JF000567.

Gilbert, G. K. (1877), Report on the geology of the Henry Mountains, 160 pp., U.S. Geogr. and Geol. Surv. of the Rocky Mt . Reg., Washington, D. C.

Harkins, N., E. Kirby, A. Heimsath, R. Robinson, and U. Reiser (2007), Transient fluvial incision in the headwaters of the Yellow River, northeastern Tibet, China, *J. Geophys. Res.*, *112*, F03S04, doi:10.1029/2006JF000570.

Hartshorn, K., N. Hovius, W. B. Dade, and R. L. Slingerland (2002), Climate-driven bedrock incision in an active mountain belt, *Science*, *297*, 2036–2038, doi:10.1126/science.1075078.

Hawk, K. L. (1992), Climatology of station storm rainfall in the continental United States: Parameters of the Bartlett-Lewis and Poisson rectangular pulses models, M.S. thesis, Mass. Inst. of Technol., Boston.

Hilley, G. E., and M. R. Strecker (2004), Steady state erosion of critical Coulomb wedges with applications to Taiwan and the Himalaya, *J. Geophys. Res.*, *109*, B01411, doi:10.1029/2002JB002284.

Howard, A. D. (1994), A detachment-limited model of drainage basin evolution, *Water Resour. Res.*, *30*(7), 2261–2285, doi:10.1029/94WR00757.

Howard, A. D., and G. Kerby (1983), Channel changes in badlands, *Geol. Soc. Am. Bull.*, *94*(6), 739–752, doi:10.1130/0016-7606(1983)94<739:CCIB>2.0.CO;2.

Istanbulluoglu, E., and R. L. Bras (2006), On the dynamics of soil moisture, vegetation, and erosion: Implications of climate variability and change, *Water Resour. Res.*, *42*, W06418, doi:10.1029/2005WR004113.

Jansen, J. D. (2006), Flood magnitude-frequency and lithologic control on bedrock river incision in post-orogenic terrain, *Geomorphology*, *82*(1–2), 39–57, doi:10.1016/j.geomorph.2005.08.018.

Jansen, J. D., D. Fabel, P. Bishop, S. Xu, C. Schnabel, and A. T. Codilean (2011), Does decreasing paraglacial sediment supply slow knickpoint retreat?, *Geology*, *39*(6), 543–546, doi:10.1130/G32018.1.

Johnson, J. P. L., and K. X. Whipple (2010), Evaluating the controls of shear stress, sediment supply, alluvial cover, and channel morphology on experimental bedrock incision rate, *J. Geophys. Res.*, *115*, F02018, doi:10.1029/2009JF001335.

Johnson, J. P. L., K. X. Whipple, L. S. Sklar, and T. C. Hanks (2009), Transport slopes, sediment cover, and bedrock channel incision in the Henry Mountains, Utah, *J. Geophys. Res.*, *114*, F02014, doi:10.1029/2007JF000862.

Kean, J. W., and J. D. Smith (2004), Flow and boundary shear stress in channels with woody bank vegetation, in *Riparian Vegetation and Fluvial Geomorphology*, *Water Sci. Appl. Ser.*, vol. 8, edited by S. J. Bennett and A. Simon, pp. 237–252, AGU, Washington, D. C., doi:10.1029/008WSA17.

Kirby, E., and K. X. Whipple (2001), Quantifying differential rock-uplift rates via stream profile analysis, *Geology*, *29*(5), 415–418, doi:10.1130/0091-7613(2001)029<0415:QDRURV>2.0.CO;2.

Lague, D. (2010), Reduction of long-term bedrock incision efficiency by short-term alluvial cover intermittency, *J. Geophys. Res.*, *115*, F02011, doi:10.1029/2008JF001210.

Lague, D., N. Hovius, and P. Davy (2005), Discharge, discharge variability, and the bedrock channel profile, *J. Geophys. Res.*, *110*, F04006, doi:10.1029/2004JF000259.

Lamb, M. P., W. E. Dietrich, and L. S. Sklar (2008), A model for fluvial bedrock incision by impacting suspended and bed load sediment, *J. Geophys. Res.*, *113*, F03025, doi:10.1029/2007JF000915.

Langbein, W. B., and S. A. Schumm (1958), Yield of sediment in relation to mean annual precipitation, *Eos Trans. AGU*, *39*(6), 1076–1084.

Lavé, J., and J. P. Avouac (2001), Fluvial incision and tectonic uplift across the Himalayas of central Nepal, *J. Geophys. Res.*, *106*(B11), 26,561–26,591, doi:10.1029/2001JB000359.

Lavé, J., and D. W. Burbank (2004), Denudation processes and rates in the Transverse Ranges, southern California: Erosional response of a transitional landscape to external and anthropogenic forcing, *J. Geophys. Res.*, *109*, F01006, doi:10.1029/2003JF000023.

Malamud, B. D., and D. L. Turcotte (2006), The applicability of power-law frequency statistics to foods, *J. Hydrol.*, *322*(1–4), 168–180, doi:10.1016/j.jhydrol.2005.02.032.

Meyer-Peter, E., and R. Müller (1948), Formulas for bed-load transport, paper presented at Second Congress, Int. Assoc. for Hydraul. Struct. Res., Stockholm.

Molnar, P. (2001), Climate change, flooding in arid environments, and erosion rates, *Geology*, *29*(12), 1071–1074, doi:10.1130/0091-7613(2001)029<1071:CCFIAE>2.0.CO;2.

Molnar, P., R. S. Anderson, G. Kier, and J. Rose (2006), Relationships among probability distributions of stream discharges in floods, climate, bed load transport, and river incision, *J. Geophys. Res.*, *111*, F02001, doi:10.1029/2005JF000310.

Montgomery, D. R., and K. B. Gran (2001), Downstream variations in the width of bedrock channels, *Water Resour. Res.*, *37*(6), 1841–1846, doi:10.1029/2000WR900393.

Newman, M. E. J. (2005), Power laws, Pareto distributions and Zipf's law, *Contemp. Phys.*, *46*(5), 323–351, doi:10.1080/00107510500052444.

Ouimet, W. B., K. X. Whipple, and D. E. Granger (2009), Beyond threshold hillslopes: Channel adjustment to base-level fall in tectonically active mountain ranges, *Geology*, *37*(7), 579–582, doi:10.1130/G30013A.1.

Paola, C., P. L. Heller, and C. L. Angevine (1992), The large-scale dynamics of grain-size variation in alluvial basins, 1: Theory, *Basin Res.*, *4*, 73–90, doi:10.1111/j.1365-2117.1992.tb00145.x.

Riebe, C. S., J. W. Kirchner, D. E. Granger, and R. C. Finkel (2001), Minimal climatic control on erosion rates in the Sierra Nevada, *Calif. Geol.*, *29*(5), 447–450.

Roe, G. H., D. R. Montgomery, and B. Hallet (2002), Effects of orographic precipitation variations on the concavity of steady-state river profiles, *Geology*, *30*(2), 143–146, doi:10.1130/0091-7613(2002)030<0143:EOOPVO>2.0.CO;2.

Roe, G. H., K. X. Whipple, and J. K. Fletcher (2008), Feedbacks among climate, erosion, and tectonics in a critical wedge orogen, *Am. J. Sci.*, *308*(7), 815–842, doi:10.2475/07.2008.01.

Safran, E. B., P. R. Bierman, R. Aalto, T. Dunne, K. X. Whipple, and M. Caffee (2005), Erosion rates driven by channel network incision in the Bolivian Andes, *Earth Surf. Process. Landf.*, *30*(8), 1007–1024, doi:10.1002/esp.1259.

Sklar, L., and W. E. Dietrich (1998), River longitudinal profiles and bedrock incision models: Stream power and the influence of sediment supply, in *Rivers Over Rock: Fluvial Processes in Bedrock Channels*, edited by K. J. Tinkler and E. E. Wohl, pp. 237–260, AGU, Washington, D. C., doi:10.1029/GM107p0237.

Sklar, L., and W. E. Dietrich (2001), Sediment and rock strength controls on river incision into bedrock, *Geology*, *29*(12), 1087–1090, doi:10.1130/0091-7613(2001)029<1087:SARSCO>2.0.CO;2.

Sklar, L. S., and W. E. Dietrich (2004), A mechanistic model for river incision into bedrock by saltating bed load, *Water Resour. Res.*, *40*, W06301, doi:10.1029/2003WR002496.

Sklar, L. S., and W. E. Dietrich (2006), The role of sediment in controlling steady-state bedrock channel slope: Implications of the saltation-abrasion incision model, *Geomorphology*, *82*(1–2), 58–83, doi:10.1016/j.geomorph.2005.08.019.

Snyder, N. P., K. X. Whipple, G. E. Tucker, and D. J. Merritts (2003a), Channel response to tectonic forcing: Field analysis of stream morphology and hydrology in the Mendocino triple junction region, northern California, *Geomorphology*, *53*(1–2), 97–127, doi:10.1016/S0169-555X(02)00349-5.

Snyder, N. P., K. X. Whipple, G. E. Tucker, and D. J. Merritts (2003b), Importance of a stochastic distribution of floods and erosion thresholds in the bedrock river incision problem, *J. Geophys. Res.*, *108*(B2), 2117, doi:10.1029/2001JB001655.

Spotila, J. A., M. A. House, A. E. Blythe, N. A. Niemi, and G. C. Bank (2002), Controls on the erosion and geomorphic evolution of the San Bernardino and San Gabriel Mountains, southern California, *Geol. Soc. Am. Spec. Pap.*, *365*, 205–230.

Stark, C. P. (2006), A self-regulating model of bedrock river channel geometry, *Geophys. Res. Lett.*, *33*, L04402, doi:10.1029/2005GL023193.

Stolar, D. B., S. D. Willett, and G. H. Roe (2006), Climatic and tectonic forcing of a critical orogen, *Geol. Soc. Am. Spec. Pap.*, *398*, 241–250, doi:10.1130/2006.2398(14).

Stolar, D., G. Roe, and S. Willett (2007), Controls on the patterns of topography and erosion rate in a critical orogen, *J. Geophys. Res.*, *112*, F04002, doi:10.1029/2006JF000713.

Tomkin, J. H., and G. H. Roe (2007), Climate and tectonic controls on glaciated critical-taper orogens, *Earth Planet. Sci. Lett.*, *262*(3–4), 385–397, doi:10.1016/j.epsl.2007.07.040.

Tomkin, J. H., M. T. Brandon, F. J. Pazzaglia, J. R. Barbour, and S. D. Willett (2003), Quantitative testing of bedrock incision models for the Clearwater River, NW Washington state, *J. Geophys. Res.*, *108*(B6), 2308, doi:10.1029/2001JB000862.

Tressler, C., J. Pederson, and R. Mackley (2010), The hunt for knickzones and their meaning along the Colorado—Signatures of transience after integration, bed resistance, or differential uplift?, paper presented at Origin and Evolution of the Colorado River System II Workshop, U.S. Geol. Surv., Flagstaff, Ariz., 24–26 May.

Tucker, G. E. (2004), Drainage basin sensitivity to tectonic and climatic forcing: Implications of a stochastic model for the role of entrainment and erosion thresholds, *Earth Surf. Process. Landf.*, *29*, 185–205, doi:10.1002/esp.1020.

Tucker, G. E., and R. L. Bras (2000), A stochastic approach to modeling the role of rainfall variability in drainage basin evolution, *Water Resour. Res.*, *36*(7), 1953–1964, doi:10.1029/2000WR900065.

Tucker, G. E., and G. R. Hancock (2010), Modelling landscape evolution, *Earth Surf. Process. Landf.*, *35*(1), 28–50, doi:10.1002/esp.1952.

Turcotte, D. L., and L. Greene (1993), A scale-invariant approach to flood-frequency analysis, *Stochastic Hydrol. Hydraul.*, *7*(1), 33–40, doi:10.1007/BF01581565.

Turowski, J. M. (2009), Stochastic modeling of the cover effect and bedrock erosion, *Water Resour. Res.*, *45*, W03422, doi:10.1029/2008WR007262.

Turowski, J. M., D. Lague, and N. Hovius (2007), Cover effect in bedrock abrasion: A new derivation and its implications for the modeling of bedrock channel morphology, *J. Geophys. Res.*, *112*, F04006, doi:10.1029/2006JF000697.

Turowski, J. M., N. Hovius, A. Wilson, and M. J. Horng (2008), Hydraulic geometry, river sediment and the definition of bedrock channels, *Geomorphology*, *99*(1–4), 26–38, doi:10.1016/j.geomorph.2007.10.001.

Turowski, J. M., D. Lague, and N. Hovius (2009), Response of bedrock channel width to tectonic forcing: Insights from a numerical model, theoretical considerations, and comparison with field data, *J. Geophys. Res.*, *114*, F03016, doi:10.1029/2008JF001133.

Valla, P. G., P. A. van der Beek, and D. Lague (2010), Fluvial incision into bedrock: Insights from morphometric analysis and numerical modeling of gorges incising glacial hanging valleys (Western Alps, France), *J. Geophys. Res.*, *115*, F02010, doi:10.1029/2008JF001079.

Whipple, K. X. (2004), Bedrock rivers and the geomorphology of active orogens, *Annu. Rev. Earth Planet. Sci.*, *32*, 151–185, doi:10.1146/annurev.earth.32.101802.120356.

Whipple, K. X. (2009), The influence of climate on the tectonic evolution of mountain belts, *Nat. Geosci.*, *2*(10), 730, doi:10.1038/ngeo638.

Whipple, K. X., and B. J. Meade (2004), Controls on the strength of coupling among climate, erosion, and deformation in two-sided, frictional orogenic wedges at steady state, *J. Geophys. Res.*, *109*, F01011, doi:10.1029/2003JF000019.

Whipple, K. X., and B. J. Meade (2006), Orogen response to changes in climatic and tectonic forcing, *Earth Planet. Sci. Lett.*, *243*(1–2), 218–228, doi:10.1016/j.epsl.2005.12.022.

Whipple, K. X., and G. E. Tucker (1999), Dynamics of the stream-power river incision model: Implications for height limits of mountain ranges, landscape response timescales, and research needs, *J. Geophys. Res.*, *104*(B8), 17,661–17,674, doi:10.1029/1999JB900120.

Whipple, K. X., and G. E. Tucker (2002), Implications of sediment-flux-dependent river incision models for landscape evolution, *J. Geophys. Res.*, *107*(B2), 2039, doi:10.1029/2000JB000044.

Whipple, K. X., G. S. Hancock, and R. S. Anderson (2000), River incision into bedrock: Mechanics and relative efficacy of plucking, abrasion, and cavitation, *Geol. Soc. Am. Bull.*, *112*(3), 490–503, doi:10.1130/0016-7606(2000)112<490:RIIBMA>2.0.CO;2.

Whittaker, A. C., P. A. Cowie, M. Attal, G. E. Tucker, and G. P. Roberts (2007), Contrasting transient and steady-state rivers crossing active normal faults: New field observations from the Central Apennines, Italy, *Basin Res.*, *19*(4), 529–556, doi:10.1111/j.1365-2117.2007.00337.x.

Willett, S. D. (1999), Orogeny and orography: The effects of erosion on the structure of mountain belts, *J. Geophys. Res.*, *104*(B12), 28,957–28,981, doi:10.1029/1999JB900248.

Willett, S. D. (2010), Late Neogene erosion of the Alps: A climate driver?, *Annu. Rev. Earth Planet. Sci.*, *38*, 411–437, doi:10.1146/annurev-earth-040809-152543.

Wobus, C., K. X. Whipple, E. Kirby, N. Snyder, J. Johnson, K. Spyropolou, B. Crosby, and D. Sheehan (2006a), Tectonics from topography: Procedures, promise, and pitfalls, *Geol. Soc. Am. Spec. Pap.*, *398*, 55–74, doi:10.1130/2006.2398(04).

Wobus, C. W., G. E. Tucker, and R. S. Anderson (2006b), Self-formed bedrock channels, *Geophys. Res. Lett.*, *33*, L18408, doi:10.1029/2006GL027182.

Wobus, C. W., J. W. Kean, G. E. Tucker, and R. S. Anderson (2008), Modeling the evolution of channel shape: Balancing computational efficiency with hydraulic fidelity, *J. Geophys. Res.*, *113*, F02004, doi:10.1029/2007JF000914.

Wohl, E., and G. C. L. David (2008), Consistency of scaling relations among bedrock and alluvial channels, *J. Geophys. Res.*, *113*, F04013, doi:10.1029/2008JF000989.

Wolman, M. G., and J. P. Miller (1960), Magnitude and frequency of forces in geomorphic processes, *J. Geol.*, *68*, 54–74, doi:10.1086/626637.

Yanites, B. J., and G. E. Tucker (2010), Controls and limits on bedrock channel geometry, *J. Geophys. Res.*, *115*, F04019, doi:10.1029/2009JF001601.

Zhang, P. Z., P. Molnar, and W. R. Downs (2001), Increased sedimentation rates and grain sizes 2–4 Myr ago due to the influence of climate change on erosion rates, *Nature*, *410*, 891–897, doi:10.1038/35069099.

R. A. DiBiase and K. X. Whipple, School of Earth and Space Exploration, Arizona State University, Tempe, AZ 85287, USA. (roman.dibiase@asu.edu)